

Disc-Jet Coupling in the Terzan 5 Neutron Star X-ray Binary EXO 1745–248

A.J. Tetarenko,^{1*} A. Bahramian,¹ G.R. Sivakoff,¹ E. Tremou,² M. Linares,^{3,4,5} V. Tudor,⁶ J.C.A Miller-Jones,⁶ C.O. Heinke,¹ L. Chomiuk,² J. Strader,² D. Altamirano,⁷ N. Degenaar,^{8,9} T. Maccarone,¹⁰ A. Patruno,^{11,12} A. Sanna,¹³ and R. Wijnands⁹

¹Department of Physics, University of Alberta, CCIS 4-181, Edmonton, AB T6G 2E1, Canada

²Department of Physics and Astronomy, Michigan State University, East Lansing, MI 48824, USA

³Instituto de Astrofísica de Canarias, c/ Vía Láctea s/n, E-38205 La Laguna, Tenerife, Spain

⁴Departamento de Astrofísica, Universidad de la Laguna, La Laguna, E-38205, S/C de Tenerife, Spain

⁵Institutt for fysikk, NTNU, Trondheim, Norway

⁶International Centre for Radio Astronomy Research- Curtin University, GPO Box U1987, Perth, WA 6845, Australia

⁷Physics and Astronomy, University of Southampton, Southampton, Hampshire SO17 1BJ, UK

⁸Institute of Astronomy, University of Cambridge, Madingley Road, Cambridge CB3 0HA, UK

⁹Anton Pannekoek Institute for Astronomy, University of Amsterdam, Science Park 904, 1098 XH, Amsterdam, The Netherlands

¹⁰Department of Physics, Texas Tech University, Box 41051, Lubbock, TX 79409-1051, USA

¹¹Leiden Observatory, Leiden University, Neils Bohrweg 2, 2333 CA, Leiden, The Netherlands

¹²ASTRON, the Netherlands Institute for Radio Astronomy, Postbus 2, 7900 AA, Dwingeloo, the Netherlands

¹³Dipartimento di Fisica, Università degli Studi di Cagliari, SP Monserrato-Sestu km 0.7, 09042 Monserrato, Italy

Accepted XXX. Received YYY; in original form ZZZ

ABSTRACT

We present the results of VLA, ATCA, and Swift XRT observations of the 2015 outburst of the transient neutron star X-ray binary (NSXB), EXO 1745–248, located in the globular cluster Terzan 5. Combining (near-) simultaneous radio and X-ray measurements we measure a correlation between the radio and X-ray luminosities of $L_R \propto L_X^\beta$ with $\beta = 1.68_{-0.09}^{+0.10}$, linking the accretion flow (probed by X-ray luminosity) and the compact jet (probed by radio luminosity). While such a relationship has been studied in multiple black hole X-ray binaries (BHXBs), this work marks only the third NSXB with such a measurement. Constraints on this relationship in NSXBs are strongly needed, as comparing this correlation between different classes of XB systems is key in understanding the properties that affect the jet production process in accreting objects. Our best fit disc-jet coupling index for EXO 1745–248 is consistent with the measured correlation in NSXB 4U 1728–34 ($\beta = 1.5 \pm 0.2$) but inconsistent with the correlation we fit using the most recent measurements from the literature of NSXB Aql X-1 ($\beta = 0.76_{-0.15}^{+0.14}$). While a similar disc-jet coupling index appears to hold across multiple BHXBs in the hard accretion state, this does not appear to be the case with the three NSXBs measured so far. Additionally, the normalization of the EXO 1745–248 correlation is lower than the other two NSXBs, making it one of the most radio faint XBs ever detected in the hard state. We also report the detection of a type-I X-ray burst during this outburst, where the decay timescale is consistent with hydrogen burning.

Key words: globular clusters: individual: Terzan 5 — ISM: jets and outflows — radio continuum: stars — stars: individual (EXO 1745–248) — stars: neutron — X-rays: binaries

1 INTRODUCTION

The accretion process onto compact objects and the production of relativistic jets are fundamentally connected. Low mass X-ray binaries (XBs), which contain a stellar-mass compact object, such as

a black hole (BH) or neutron star (NS), accreting from a companion star, are ideal candidates to study this relationship, as the rapid (day–week) outburst timescales of these systems allow us to track accretion and jet behaviour in real time.

Multi-wavelength studies of XBs have linked changes in the accretion flow (probed by spectral and variability properties of the X-ray emission) to those in the jet (probed by radio emission, e.g.,

* E-mail: tetarenk@ualberta.ca

Migliari & Fender 2006; Tudose et al. 2009; Miller-Jones et al. 2012; Corbel et al. 2013). In BHXB systems, a phenomenological model has been put forward to explain this connection, where changes in mass accretion rate are the catalyst driving changes in jet behaviour (Tananbaum et al. 1972; Blandford & Konigl 1979; Vadawale et al. 2003; Fender et al. 2004a, 2009). In the hard X-ray accretion state an optically-thick, steady, compact jet is present. As the mass accretion rate increases during the rise of the outburst, the jet velocity and power are also thought to increase (although this has not yet been directly proven from observational data, as measurements of jet velocity in the hard state are difficult to make). When the source makes the transition from hard to soft accretion states at higher luminosities, the system launches discrete, optically-thin, relativistically-moving ejecta, possibly as a result of internal shocks in the jet flow produced by the changes in jet velocity. The compact jet is quenched as the source moves into the softer accretion state, and then re-established as the source moves back into the hard state (where the jet is re-established well before quiescence; Kalemci et al. 2013).

Similar to BHXBs, NSXB outburst behaviour is also thought to be governed by mass accretion rate (e.g., Homan et al. 2010). In terms of the connection between inflow and outflow, NSXB and BHXB systems display both similarities and differences (Migliari & Fender 2006). A steady, compact jet is observed in NSXBs at lower X-ray luminosities ($< 0.1 L_{\text{edd}}$) in hard accretion states (i.e., island accretion states; Migliari et al. 2010), and discrete jet ejections have been found at higher X-ray luminosities (typically seen in Z sources persistently accreting at high fractions of Eddington; e.g., Fender et al. 2004b, Fomalont et al. 2001; Spencer et al. 2013), as seen in BHXBs. However, BHXBs tend to be much more radio loud than NSXBs at the same X-ray luminosity (Fender & Kuulkers 2001; Migliari & Fender 2006). While this could imply NS jets are less powerful, Kording et al. (2006) suggest that jet power is comparable in NS/BH systems, and properties such as the mass of the compact object or radiative efficiency are responsible for the different radio luminosity levels. Additionally, NSXB jets do not all appear to be fully quenched in softer accretion states as they are in BHXBs (Migliari et al. 2004). While commonalities could indicate that the physical mechanism (possibly related to the mass accretion rate) powering the jets in both classes of system is similar, differences suggest the nature of the compact object still may play an important role. Analyzing and quantifying the similarities and differences between these systems is key to understanding the properties that affect the jet production process (e.g., mass, spin, existence of a surface or event horizon) across all scales.

A key observational tracer of the accretion-jet connection in XBs is the correlation found between radio and X-ray luminosities in the hard state ($L_R \propto L_X^\beta$, where β represents the disc-jet coupling index, e.g., $\beta_{\text{BH}} \sim 0.6$; Corbel et al. 2003; Gallo et al. 2003; Corbel et al. 2013)¹. This non-linear correlation is consistent with scale-invariant jet models, where a self-absorbed synchrotron jet is coupled to an accretion flow, total jet power is a fixed fraction of the accretion power, and X-ray luminosity depends on mass accretion rate (Falcke & Biermann 1995; Heinz & Sunyaev 2003; Markoff et al. 2003). Further, through the addition of a mass parameter, this correlation has been extended across the mass scale to in-

clude AGN, the supermassive analogues of BHXBs (Merloni et al. 2003); $\log(L_X) = \xi_R \log(\nu L_R) - \xi_M \log M_{\text{BH}} + B$, where the coefficients, $\xi_R = 1.45 \pm 0.04$, $\xi_M = 0.88 \pm 0.06$, and $B = -6.07 \pm 1.10$ (Falcke et al. 2004; Plotkin et al. 2012).

The $L_R \propto L_X^\beta$ correlation has been shown to hold in multiple BHXBs from quiescent luminosities as low as $10^{-9} L_{\text{edd}}$ to outburst luminosities as high as $10^{-2} L_{\text{edd}}$, above which the compact jet is quenched (we note that while the correlation holds tightly in individual systems, there is more scatter when the whole sample of BHXBs is considered together; Gallo et al. 2014; Plotkin et al. 2015). However, our knowledge of this correlation in individual NS systems is limited. Two NSXBs (4U 1728–34 and Aql X–1), have measured correlations, including data spanning only one order of magnitude in X-ray luminosity (Migliari & Fender 2006). While 4U 1728–34 shows a correlation of $L_R \propto L_X^{1.5}$ (Migliari et al. 2003), consistent with what we would expect from radiatively efficient accretion due to the NS’s surface, there have been conflicting results for this correlation in Aql X-1. Tudose et al. (2009) measured $L_R \propto L_X^{0.4}$ for Aql X-1, which is more consistent with radiatively inefficient accretion flows (like those seen in BHXBs). However, Tudose et al. (2009) took Aql X-1 data from a mixture of accretion states; Migliari & Fender (2006) show the correlation is consistent with $L_R \propto L_X^{1.4}$ when including only data taken in the hard accretion states for both Aql X-1 and 4U 1728–34 (we note that the Migliari & Fender (2006) correlation only included 2 data points from Aql X-1, while the data from the full hard state coverage of the outburst, presented in Miller-Jones et al. (2010), is more consistent with a flatter correlation). Including data from softer accretion states could account for the differing disc-jet coupling indices between Aql X–1 and 4U 1728–34, although we direct the reader to the discussion section of this paper for an updated correlation for Aql X-1 and discussion of this discrepancy. Further, three transitional milli-second pulsars (tMSPs; binary NS systems that have been found to switch from a rotation powered pulsar state to an accreting XB state), have recently been shown to all lie on a shallower correlation, $L_R \propto L_X^{0.7}$, distinct from hard state NSXBs and much more consistent with BHXBs (Deller et al. 2015). In addition to the disc-jet coupling index, the intrinsic normalization of this correlation clearly varies between BHXBs, NSXBs and tMSPs as groups, and between individual BHXB systems (Gallo et al. 2014). More well measured correlations, including normalization and disc-jet coupling indices are needed to determine which NSXB behaviour is the norm, and determine the mechanisms driving the difference between the correlations of hard state NSXBs and tMSPs. Here we report on the third individual NSXB radio/X-ray correlation measured to date, from data taken during the 2015 outburst of the NSXB EXO 1745–248, located in the globular cluster Terzan 5.

1.1 Terzan 5: EXO 1745–248

Terzan 5 is a massive ($\sim 10^6 M_\odot$; Lanzoni et al. 2010) globular cluster located in the Galactic centre region (distance of 5.9 ± 0.5 kpc; Valenti et al. 2007), with a high stellar density, leading to a very high stellar encounter rate (the highest measured so far; Bahramian et al. 2013). This cluster contains three transient X-ray sources confirmed to be accreting NSs, EXO 1745–248 (Terzan 5 X-1), IGR J17480–2446 (Terzan 5 X-2), and Swift J174805.3–244637 (Terzan 5 X-3; Wijnands et al. 2005; Bordas et al. 2010; Strohmayer & Markwardt 2010; Degenaar & Wijnands 2012; Bahramian et al. 2014), as well as several other detected quiescent X-ray sources (Heinke et al.

¹ We note that Coriat et al. 2011 present evidence for two different tracks in this correlation for BH systems, a radio-loud and radio-quiet track, although, recent work by Gallo et al. 2014 found that a two track description is only statistically preferred when luminosity errors are < 0.3 dex.

Table 1. Summary of Swift XRT Observations and Fluxes of EXO 1745–248

Obs ID	Exp. Time (s)	Mode	Date (2015)	MJD ^a	Count Rate (cnt s ⁻¹)	N _H (10 ²² cm ⁻²)	Γ ^b	kT ^c (keV)	F _{1–10} ^{d,e} (10 ⁻¹⁰ erg s ⁻¹ cm ⁻²)	χ _v ²	dof
Hard State											
32148017 ^f	1965.36	PC	Mar 17	57098.7491	0.73 ^{+0.03} _{-0.02}	4.41 ^{+0.85} _{-0.74}	1.12 ^{+0.22} _{-0.21}	...	3.77 ^{+0.26} _{-0.23}	1.01	44
32148021	1188.47	WT	Mar 21	57102.8797	9.11 ^{+0.19} _{-0.22}	3.36 ^{+0.20} _{-0.19}	1.24 ^{+0.08} _{-0.07}	...	14.19 ^{+0.32} _{-0.32}	1.09	117
32148023	771.57	WT	Mar 23	57104.0629	7.33 ^{+0.26} _{-0.29}	3.01 ^{+0.29} _{-0.27}	1.31 ^{+0.11} _{-0.10}	...	10.61 ^{+0.36} _{-0.34}	1.07	62
32148024 ^g	898.50	WT	Mar 25	57106.2081	9.12 ^{+0.20} _{-0.22}	3.11 ^{+0.22} _{-0.21}	1.22 ^{+0.08} _{-0.08}	...	13.73 ^{+0.36} _{-0.35}	1.09	90
32148024	323.36	WT	Mar 25	57106.2564	8.66 ^{+0.25} _{-0.27}	2.65 ^{+0.37} _{-0.33}	1.13 ^{+0.15} _{-0.14}	...	12.49 ^{+0.56} _{-0.55}	0.87	30
32148025	513.67	WT	Mar 26	57107.8624	7.84 ^{+0.24} _{-0.26}	3.17 ^{+0.38} _{-0.35}	1.20 ^{+0.14} _{-0.14}	...	11.84 ^{+0.45} _{-0.44}	1.00	44
32148025	534.59	WT	Mar 26	57107.9322	7.21 ^{+0.24} _{-0.27}	2.85 ^{+0.33} _{-0.31}	1.16 ^{+0.13} _{-0.13}	...	11.48 ^{+0.43} _{-0.43}	1.01	42
32148026	302.78	WT	Mar 28	57109.5274	7.86 ^{+0.25} _{-0.26}	2.44 ^{+0.41} _{-0.37}	0.94 ^{+0.16} _{-0.15}	...	11.79 ^{+0.56} _{-0.55}	1.29	42
32148027	344.07	WT	Apr 02	57114.4467	7.76 ^{+0.29} _{-0.33}	2.43 ^{+0.38} _{-0.35}	1.00 ^{+0.15} _{-0.15}	...	11.15 ^{+0.52} _{-0.51}	0.95	46
32148029	764.11	WT	Apr 06	57118.1135	9.47 ^{+0.25} _{-0.27}	2.09 ^{+0.20} _{-0.18}	0.87 ^{+0.08} _{-0.08}	...	13.74 ^{+0.37} _{-0.38}	1.21	80
32148030	443.32	WT	Apr 12	57124.3745	25.84 ^{+0.57} _{-0.63}	2.13 ^{+0.15} _{-0.14}	0.86 ^{+0.07} _{-0.07}	...	38.96 ^{+0.87} _{-0.86}	1.08	99
32148031	704.54	WT	Apr 13	57125.8931	12.18 ^{+0.60} _{-0.66}	2.20 ^{+0.18} _{-0.18}	0.90 ^{+0.08} _{-0.08}	...	29.05 ^{+0.74} _{-0.73}	1.04	98
32148032 ^f	849.08	PC	Apr 14	57126.4853	6.34 ^{+0.10} _{-0.09}	2.07 ^{+0.21} _{-0.20}	0.84 ^{+0.09} _{-0.09}	...	43.41 ^{+1.33} _{-1.31}	1.11	48
Soft State^h											
32148033	615.82	WT	Apr 20	57132.2902	95.13 ^{+1.63} _{-1.74}	2.47 ^{+0.05} _{-0.05}	...	2.62 ^{+0.07} _{-0.06}	121.39 ^{+1.19} _{-1.19}	1.26	100
32148033	579.58	WT	Apr 20	57132.6898	110.15 ^{+1.01} _{-1.09}	3.37 ^{+0.09} _{-0.09}	1.53 ^{+0.04} _{-0.04}	...	158.37 ^{+1.96} _{-1.91}	1.38	107
32148034	385.78	WT	Apr 22	57134.1423	106.36 ^{+1.15} _{-1.20}	2.44 ^{+0.06} _{-0.06}	...	3.76 ^{+0.18} _{-0.16}	140.70 ^{+1.76} _{-1.75}	1.35	45
32148034	290.99	WT	Apr 22	57134.2161	113.53 ^{+1.26} _{-1.39}	2.95 ^{+0.15} _{-0.14}	0.93 ^{+0.06} _{-0.06}	...	184.63 ^{+3.01} _{-2.96}	0.93	36
32148035	376.85	WT	Apr 24	57136.4053	80.21 ^{+1.10} _{-1.17}	3.37 ^{+0.17} _{-0.16}	1.53 ^{+0.07} _{-0.07}	...	112.37 ^{+2.27} _{-2.18}	1.32	31
32148036	988.60	WT	Apr 26	57138.1412	66.57 ^{+1.12} _{-1.20}	2.52 ^{+0.05} _{-0.05}	...	3.13 ^{+0.09} _{-0.09}	81.7 ^{+0.08} _{-0.08}	1.41	71
Hard State											
32148053	1106.30	WT	Jun 21	57194.6817	0.14 ^{+0.03} _{-0.04}	1.66 ^{+1.17} _{-0.84}	1.44 ^{+0.74} _{-0.62}	...	0.32 ^{+0.06} _{-0.05}	1.19	9
32148054 ⁱ	79.91	WT	Jun 24	57197.8643	0.09 ^{+0.06} _{-0.03}	0.09 ^{+0.11} _{-0.06}

^a All MJD values quoted represent the mid point of the observations.

^b Γ represents the power-law photon index.

^c T represents the DISKBB temperature.

^d Uncertainties are quoted at the 1σ level.

^e 1–10 keV flux; see footnote 11 for discussion of why this X-ray band is chosen.

^f Note that this observation was piled-up; please see §2.1 for details.

^g Note that this observation contained an X-ray burst; please see §2.1 & 4.2 for details. We excluded the burst interval when performing our spectral analysis of this observation.

^h Note that soft state measurements are not included in our radio/X-ray correlation analysis. We show them here for comparison purposes and to clearly show the transition between the hard and soft state.

ⁱ Due to the limited exposure time of this observation, the flux for this observation is determined by using the model fits from the previous observation.

2006). Historically, X-ray activity was first detected from Terzan 5 in 1980, in the form of multiple X-ray bursts, indicating the presence of an outbursting NSXB (Makishima et al. 1981; Inoue et al. 1984). Subsequent X-ray activity was observed in 1984, 1990, 1991, 2000, 2002, 2010, 2011, and 2012, where activity in 2000 and 2011² was attributed to EXO 1745–248³ (Heinke et al. 2003; Altamirano et al. 2012b; Serino et al. 2012; see Table 1 in Degenaar & Wijnands 2012 and references therein for a review of past X-ray activity in Terzan 5).

² The 2011 outburst showed superburst activity (Altamirano et al. 2012a).

³ We note that it is not known whether the Terzan 5 outbursts in the early 80s and 90s are associated with EXO 1745–248.

On 2015 March 13, renewed X-ray activity from Terzan 5 was detected (Altamirano et al. 2015) by the Swift Burst Alert Telescope (BAT; Krimm et al. 2013) transient monitor. While the X-ray position from follow up Swift X-ray Telescope (XRT) observations (Bahramian et al. 2015) was consistent with EXO 1745–248, IGR J17480–2446, and several other quiescent X-ray sources (Heinke et al. 2006), the spectrum showed a higher than typical hydrogen column density, $N_H = 4 \pm 0.8 \times 10^{22}$, for sources in Terzan 5 (Bahramian et al. 2014), consistent with previous observations of EXO 1745–248 (Kuulkers et al. 2003). Linares et al. (2015) measured a refined Swift XRT source position centered on the known X-ray position of EXO 1745–248 (2′.2 error circle) further suggesting that the outbursting source in Terzan 5 was in fact EXO 1745–248. Tremou et al. (2015) detected a radio counterpart with

Table 2. Summary of Radio Frequency Observations and Flux Densities of EXO 1745–248

Telescope	Date (2015)	MJD ^a	Freq. (GHz)	Flux ^{b,c} ($\mu\text{Jy bm}^{-1}$)	Spectral Index ^d
VLA	Mar 19	57100.43155	9.0	28.7±6.0	...
VLA	Mar 19	57100.43155	11.0	22.8±8.0	-1.20±1.97
VLA	Mar 24	57105.53915	9.0	47.8±6.0	...
VLA	Mar 24	57105.53915	11.0	30.3±8.0	-2.20±1.4
VLA	Apr 12	57124.40413	9.0	238.1±8.3	...
VLA	Apr 12	57124.40413	11.0	247.6±9.3	0.15±0.26
ATCA	Apr 16	57128.75694	5.5	372.0±7.0	...
ATCA	Apr 16	57128.75694	9.0	340.0±7.8	-0.18±0.06
ATCA	Jun 23	57196.60938 ^e	5.5	< 17	...
ATCA	Jun 23	57196.60938 ^e	9.0	< 19	...

^a All MJD values quoted represent the mid point of the observations.

^b Uncertainties are quoted at the 1σ level.

^c Radio flux density, where uncertainties quoted include the 1% systematic errors appropriate to both VLA X-band observations and the ATCA 3/6 cm observations.

^d All spectral indices given use the formalism, $f_\nu \propto \nu^\alpha$; where α is the spectral index.

^e The source was not detected in these observations, fluxes presented here are 3σ upper limits.

observations by the Karl G. Jansky Very Large Array (VLA). These radio observations, which localized the source within $0''.4$ of the published Chandra coordinates (source CX3 in [Heinke et al. 2006](#)), and later optical observations that identified the optical counterpart during this outburst ([Ferraro et al. 2015](#)), confirmed the identification by [Linares et al. \(2015\)](#).

We obtained multiple epochs of (near-) simultaneous VLA, Australia Telescope Compact Array (ATCA), and Swift XRT observations during the 2015 outburst of EXO 1745–248. In §2 we describe the data collection and reduction processes. In §3 we present a refined radio position of EXO 1745–248, measurements of the jet spectral index, and the radio/X-ray correlation in this source. §4 contains an interpretation of this correlation, comparison to other NS and BH XB sources, and an analysis of an X-ray burst detected in one of the Swift XRT observations. A summary of the results is presented in §5.

2 OBSERVATIONS AND DATA ANALYSIS

2.1 X-ray Observations

We monitored the outburst of EXO 1745–248 multiple times per week with Swift XRT following its detection in 2015. This paper considers only those observations that are most relevant to analyzing the radio/X-ray correlation and accretion state transition. We summarize these observations in Table 1 and Figure 1; these consist of two observations in photon counting (PC) mode, which produces 2D images, and 19 observations in windowed timing (WT) mode, which collapses data to 1-dimension for fast readout.

We used HEASOFT 16.6 and FTOOLS ⁴ ([Blackburn 1995](#)) for all data reduction and analysis. All Swift XRT observations were reprocessed via `xrtpipeline` and `xselect` was used to manually extract source and background spectra. We used

`xrtmkarf` to produce ancillary response files. Finally, we performed spectral analysis using XSPEC 12.8.2 ([Arnaud 1996](#)) in the 0.3–10 keV band for PC mode data and the 0.6–10 keV band for WT mode data.

Our PC mode observations in this campaign were heavily piled-up due to the high count rate of the source. Thus we followed the UK Swift Science Data Centre pile-up thread⁵ and extracted source spectra from an annulus (13–70" for the first PC mode observation and 20–100" for the second PC observation), excluding the piled-up region in these observations. The PC mode observations only showed evidence for one bright source.

For heavily absorbed sources, WT data show low energy spectral residuals, which can cause spectral uncertainties in the ≤ 1.0 keV region⁶. These residuals mostly affect grade 1 events and above, and events below ~ 0.6 keV. Thus for our WT mode data, we extracted spectra only from grade 0 events and excluded events below 0.6 keV.

We extracted a spectrum from each observation separately and performed spectral fitting. Our main model for spectral analysis is an absorbed powerlaw (TBABS*PEGPOWERLAW in XSPEC), where we assume the cross sections from [Verner et al. \(1996\)](#) and abundances from [Wilms et al. \(2000\)](#). We use a comparison of Swift/BAT and MAXI light curves (Figure 1) to aid in defining which observations are in the hard/soft accretion state. This comparison reveals a large drop in the hard flux simultaneous with a rise in the soft flux, indicative of a hard-to-soft state transition on MJD 57131. Thus for spectra from Swift/XRT observations after this point, we tried both absorbed powerlaw and absorbed disc blackbody (TBABS*DISKBB in XSPEC) models, and chose the fit with lower χ^2 for this study. Although a two-component model (e.g., DISKBB+PEGPOWERLAW) is often used to fit NSXB soft states, we are only interested in identifying the dominant component (as opposed to performing a detailed characterization of the spectrum)

⁴ <http://heasarc.gsfc.nasa.gov/ftools/>

⁵ <http://www.swift.ac.uk/analysis/xrt/pileup.php>

⁶ http://www.swift.ac.uk/analysis/xrt/digest_cal.php#abs

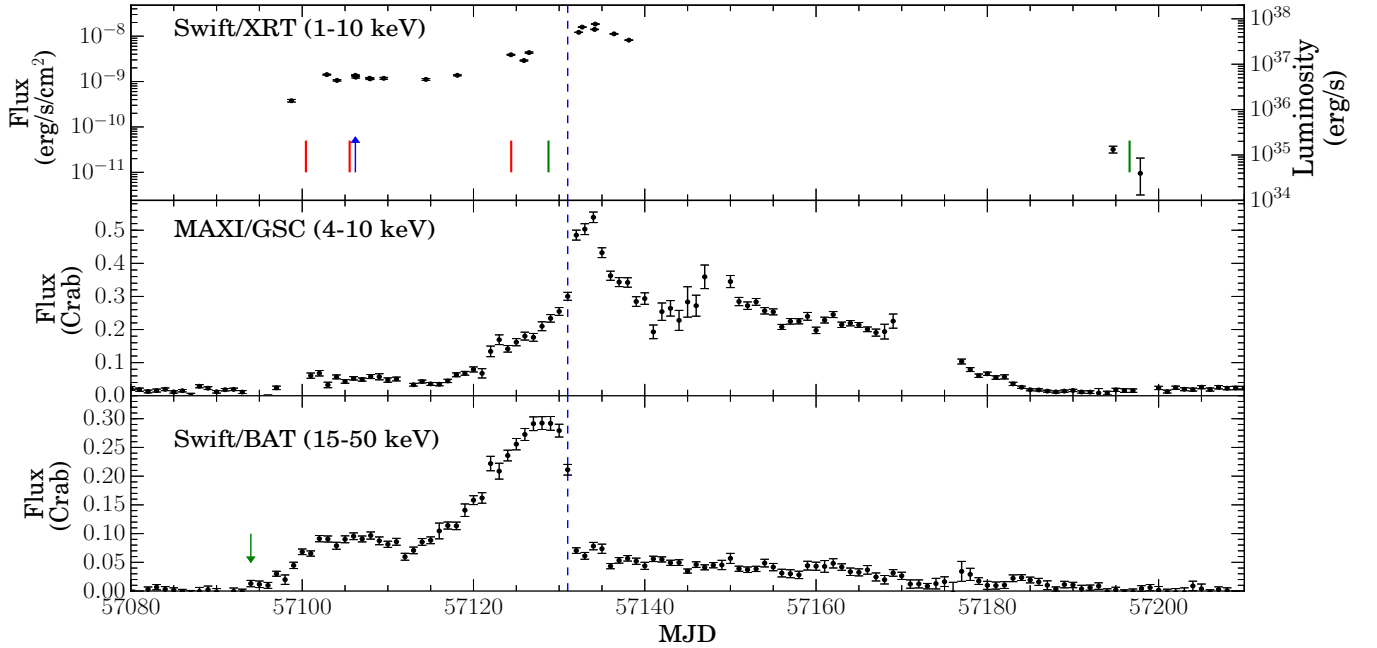


Figure 1. X-ray light curves of the 2015 outburst from EXO 1745–248 as seen by Swift/XRT (top), MAXI/GSC (middle; <http://maxi.riken.jp>) and Swift/BAT (bottom; [Krimm et al. 2013](#)). Swift/XRT fluxes are derived from spectral fitting (see §2.1 in text). To calculate luminosity in the top panel, we assumed a distance of 5.9 kpc. The blue dashed line shows the apparent hard to soft state-transition at MJD 57131. Vertical bars in the top panel indicate the time of radio observations by the ATCA (green) and VLA (red). The blue arrow in the top panel indicates the time of the detected X-ray burst, and the green arrow in the bottom panel indicates the time of the first detection of the outburst in Swift BAT. Note that while we only use the hard state measurements in our radio/X-ray correlation analysis, we show some of the soft state measurements near the times of our radio observations to clearly show the hard-soft transition and the luminosity at that transition.

and obtaining a flux estimate. Thus we only fit simple one component models for the purpose of this work.

We note that the MAXI and Swift/BAT data do not clearly show the soft-to-hard state transition, probably because it occurred at a lower luminosity where the S/N of these instruments is low. However, all observed XB outbursts return to the hard state at luminosities above 10^{35} erg s $^{-1}$ ([Maccarone 2003](#); [Tetarenko et al. 2016](#)), so we conclude it is extremely likely that the last two Swift data points, and the ATCA measurement between them, occurred during the hard state. The power law index measured for the June 21 observation, which was more consistent with the hard state observations than the soft state observations, support this conclusion. Swift/XRT observations and results of our spectral analysis are reported in Table 1.

We also detected an X-ray burst during the Mar 25 observation, which is discussed in detail in §4.2.

2.2 Radio Observations

2.2.1 VLA

Terzan 5 was observed with the VLA (Project Code: 14B-216) in three epochs, 2015 March 19, March 24, and April 12. The array was in the B configuration, with a resolution of $0''.6$, and we had 25.9 min on source for each epoch. All observations were made with the 3-bit samplers in X band (8 – 12 GHz), comprised of 2

base-bands, each with 16 spectral windows of 64 2-MHz channels each, giving a total bandwidth of 2.048 GHz per base-band. Flagging, calibration and imaging of the data were carried out within the Common Astronomy Software Application package (CASA⁷; [McMullin et al. 2007](#)) using standard procedures. When imaging we used a natural weighting scheme to maximize sensitivity, two Taylor terms (nterms=2) to account for the large fractional bandwidth, and did not perform any self-calibration. We used 3C286 (J1331+305) as a flux calibrator and J1751–2524 as a phase calibrator. Flux densities of the source were measured by fitting a point source in the image plane (Stokes I with the IMFIT task), and, as is standard for VLA X band data, systematic errors of 1% were added. All flux density measurements are reported in Table 2.

2.2.2 ATCA

During the 2015 outburst of EXO 1745–248, Terzan 5 was observed with the ATCA (Project Code: C2877) in two epochs, 2015 April 16 and June 23. The array was in the 6A configuration (resolution of $1''.89/1''.16$ arcsec at 5.5/9 GHz) in the first epoch, and the 6D configuration (resolution of $1''.91/1''.16$ arcsec at 5.5/9 GHz) in the second epoch. We had 8.0 hrs on source for both epochs. All observations were carried out at 5.5 and 9 GHz simultaneously,

⁷ <http://casa.nrao.edu>

where each frequency band is comprised of 2048 1-MHz channels, giving a total bandwidth of 2.048 GHz per frequency band. Flagging and calibration were carried out with the Multichannel Image Reconstruction, Image Analysis and Display (MIRIAD) software (Sault et al. 1995), using standard procedures. We used 1934-638 as a flux calibrator and 1748-253 as a phase calibrator. Imaging of the data was carried out within CASA using a Briggs weighting scheme (robust=1) and two Taylor terms (nterms=2). We did not perform any self-calibration. Flux densities of the source were measured by fitting a point source in the image plane (Stokes I with the IMFIT task), and, as is standard for ATCA data, systematic errors of 1% were added. All flux density measurements are reported in Table 2.

3 RESULTS

3.1 Radio Source Position

Through stacking all three epochs of our VLA data in the uv -plane, we measure a refined radio position of EXO 1745–248 to be the following (J2000),

$$\begin{aligned} \text{RA} : & \quad 17^{\text{h}}48^{\text{m}}05^{\text{s}}.22467 \pm 0.00084 \pm 0.01 \\ \text{DEC} : & \quad -24^{\circ}46'47''.666 \pm 0.033 \pm 0.06 \end{aligned}$$

where the quoted error bars represent the statistical error from fitting in the image plane and the nominal systematic uncertainties of 10% of the beam size, respectively.

This source position is within $0'.33$ of the published X-ray location of EXO 1745-248 (CX 3 in Heinke et al. 2006; RA/DEC errors 0.002s/0.02 arcsec), and within $0'.10$ of the optical location of EXO 1745-248 (Ferraro et al. 2015; RA/DEC errors 0.01s/0.2 arcsec). The radio source is clearly unassociated with the two other previously identified NSXBs in Terzan 5; it is $2'.4$ away from IGR J17480–2446 (CX 24 in Heinke et al. 2006; RA/DEC errors 0.005s/0.09 arcsec) and $10'.3$ away from Swift J174805.3–244637 (Bahramian et al. 2014; RA/DEC errors 0.02s/0.2 arcsec).

3.2 Jet Spectral Indices

To obtain the jet spectral indices we fit (linearly in log space) a power-law to the derived radio flux densities (between the two base-bands in the VLA data and between 5.5 and 9 GHz in the ATCA data) against frequency at each epoch ($f_{\nu} \propto \nu^{\alpha}$; where α is the spectral index). All spectral index measurements are reported in Table 2. In the March 19 and April 12 VLA epochs, the spectral index measurements are consistent with a flat ($\alpha = 0$) or slightly inverted ($\alpha > 0$) spectrum, although, in the March 24 VLA epoch and the ATCA epoch on Apr 16, the spectral index appears to be more consistent with a slightly steeper index ($\alpha < 0$). However, both the March 19 and March 24 VLA epochs have large uncertainties (due to the low signal-to-noise ratio and small lever arm in frequency) that make it impossible to conclusively distinguish between steep, flat, or an inverted spectra. A flat or slightly inverted spectrum, commonly seen from compact jets during hard accretion states in BHXBs (Fender et al. 2001) and some NSXBs (e.g., Migliari & Fender 2006; Migliari et al. 2010), is believed to be produced as the result of the superposition of many different synchrotron components originating from different regions along the jet (e.g., Blandford & Konigl 1979).

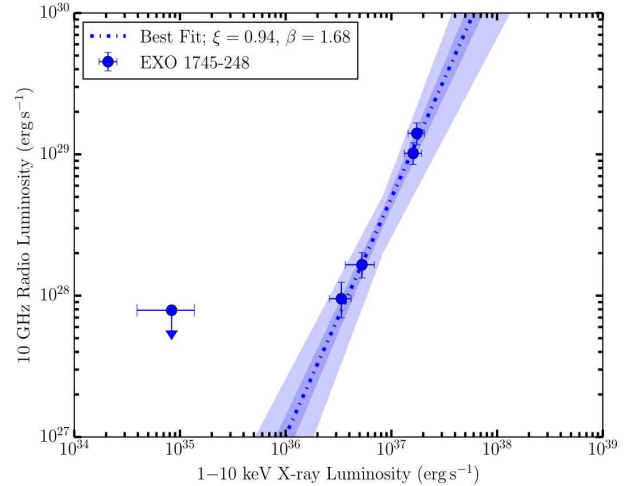


Figure 2. Radio/X-ray correlation during the hard accretion state of the 2015 outburst of EXO 1745–248. The dash-dotted line indicates the best fit using our MCMC techniques (see text for best fit parameters and uncertainties). The shaded regions represent the 1σ (dark blue) and 3σ (light blue) confidence intervals of the regression. Note that we do include the upper limit data point in our fit. The luminosities displayed here are calculated assuming a distance of 5.9 kpc.

Table 3. Radio and interpolated X-ray fluxes of EXO 1745–248 used in the radio/X-ray correlation analysis

MJD	$F_{10\text{GHz}}^{a,b}$ ($\mu\text{Jy bm}^{-1}$)	$F_{1-10\text{keV}}^{a,c}$ ($10^{-10} \text{ erg s}^{-1} \text{ cm}^{-2}$)
57100.43155	23.2 \pm 5.0	8.02 $^{+0.41}_{-0.40}$
57105.53915	40.0 \pm 4.0	12.78 $^{+0.67}_{-0.69}$
57124.40413	245.3 \pm 5.6	38.78 $^{+0.82}_{-0.89}$
57128.75694	340.0 \pm 7.8	41.89 $^{+1.39}_{-1.47}$
57196.60938 ^d	< 19	0.20 $^{+0.13}_{-0.11}$

^a Uncertainties are quoted at the 1σ level.

^b 10 GHz radio flux from combining the 2 base-bands.

^c Interpolated X-ray fluxes in the 1–10 keV band.

^d The source was not detected in this observation, the flux presented here is 3σ upper limit.

3.3 Radio X-Ray Correlation in EXO 1745–248

To fit the radio/X-ray correlation in EXO 1745–248, we use radio and X-ray luminosities (spanning ~ 1 dex in X-ray luminosity⁸) at 10 GHz (combined base-band measurements) and 1–10 keV, re-

⁸ While our radio observations span ~ 3 dex in X-ray luminosity, our lowest luminosity point only has an upper limit on radio luminosity and thus is not very constraining.

spectively⁹, and a Markov Chain Monte Carlo (MCMC¹⁰) fitting algorithm. To properly account for uncertainties in both distance (5.9 ± 0.5 kpc; Valenti et al. 2007) and flux, we build a hierarchical model within our MCMC, where we include distance as an additional parameter. This in turn allows us to calculate luminosities using our measured fluxes/uncertainties and samples drawn from the distance distribution (i.e., a Gaussian with mean of 5.9 and standard deviation of 0.5), and then perform a linear fit in log space on these luminosities. Although many previous studies only compare the X-ray measurements closest in time to the radio measurements, our method takes a more conservative approach to data that is not strictly simultaneous. In particular, as our XRT X-ray observations were not strictly simultaneous with the VLA radio observations, we use a MCMC linear interpolation method to estimate X-ray fluxes at the times of the radio observations. However, as the X-ray flux of outbursting NSXBs can vary on timescales of less than a day (the maximum separation between our radio and X-ray observations), our linear interpolation method may underestimate the uncertainties on the interpolated X-ray fluxes. Therefore, we conservatively scale the uncertainties on the interpolated X-ray fluxes to cover the full flux range of the neighbouring X-ray data (see Table 3 for radio and interpolated X-ray fluxes used in our MCMC fitting).

We follow Gallo et al. (2014) when performing our MCMC fit with the following functional form,

$$(\log L_R - \log L_{R,c}) = \log \xi + \beta(\log L_X - \log L_{X,c}) \quad (1)$$

where, L_R and L_X are radio (10 GHz) and X-ray (1–10 keV) luminosity, respectively, centering values $L_{R,c} = 3.89 \times 10^{28}$ erg s⁻¹ and $L_{X,c} = 8.38 \times 10^{36}$ erg s⁻¹ are the geometric means of the simultaneous radio and X-ray luminosity measurements (not including the upper limit data point), ξ represents the normalization constant and β represents the disc-jet coupling index. To include the upper limit data point in our fit, and better constrain the normalization and disc-jet coupling index, we add a condition in our log probability that does not allow solutions where, at the X-ray luminosity of the upper limit data point, the corresponding radio luminosity would exceed the upper limit value. Our best fit parameters are, normalization $\xi = 0.94^{+0.14}_{-0.13}$ and disc-jet coupling index $\beta = 1.68^{+0.10}_{-0.09}$, where uncertainties are quoted at the 15th and 85th percentiles (as done in Gallo et al. 2014; also see Figure 2).

4 DISCUSSION

In the framework of scale-invariant jet models coupled to an accretion flow, X-ray luminosity scales with mass accretion rate ($L_X \propto \dot{M}^q$)¹¹, total jet power is a fraction of the accretion power ($Q_{\text{jet}} =$

$f\dot{M}c^2$), and the jet luminosity scales with jet power, according to (Falcke & Biermann 1995; Heinz & Sunyaev 2003; Markoff et al. 2003),

$$L_v \propto Q_{\text{jet}}^\eta \quad (2)$$

Here, $\eta = \frac{2p-(p+6)\alpha+13}{2(p+4)}$ depends on the power-law index of the electron energy distribution (p), and the jet spectral index (α). When the jet is observed in the radio regime this in turn implies,

$$L_R \propto L_X^{\eta/q} \quad (3)$$

where radiatively efficient flows display $q = 1$, and radiatively inefficient flows display $q = 2 - 3$.

In the previous section we reported a disc-jet coupling index of $1.68^{+0.10}_{-0.09}$ for EXO 1745–248, which is consistent with a radiatively efficient accretion flow (possibly due to the neutron star surface; see Migliari & Fender 2006 and references therein for discussion) coupled to a steady, compact jet (i.e., values of $q = 1$, $2 \leq p \leq 3$, $-0.7 \leq \alpha \leq 0.1$ will produce values of $1.4 < \eta < 2.0$ within the confidence interval we derived for EXO 1745–248).

4.1 Comparison to other Neutron Star and Black Hole Systems

While several BHXBs have measured disc-jet coupling indices (e.g., Gallo et al. 2014 combine data from 24 different BHXB systems to yield a best-fit disc jet coupling index of 0.61 ± 0.03), to date there are only two individual NSXBs with previously measured disc-jet coupling indices, Aql X-1 and 4U 1728–34. Migliari et al. (2003) report a disc-jet coupling index of 1.5 ± 0.2 in 4U 1728–34, while different works report conflicting correlations for Aql X-1. The Aql X-1 data used to fit the correlation in Tudose et al. (2009) originates from mixed accretion states. While Migliari & Fender (2006) find that 4U 1728–34 and Aql X-1 are well fit together with a disc-jet coupling index of 1.40 ± 0.23 , this fit only includes two data points from Aql X-1. More recently Migliari et al. (2011) reported that Aql X-1 is fit by a disc-jet coupling index of ~ 0.6 (with no errors reported).

Therefore, we combined the most recent hard state Aql X-1 data from the literature, including the two measurements from Migliari & Fender (2006), as well as measurements from Miller-Jones et al. (2010), but excluding data with radio upper limits or hard X-ray colour¹² < 0.75 . We find a disc-jet coupling index of $0.76^{+0.14}_{-0.15}$. This new Aql X-1 result is not consistent with the 4U 1728–34 result, and suggests that the use of mixed accretion state measurements in Tudose et al. (2009) is not the sole cause of the flatter disc-jet coupling index. Instead the disc-jet coupling index of Aql X-1 is more consistent with those of BHXBs. However, this correlation in Aql X-1 is only measured over ~ 0.8 dex, and we note that Corbel et al. (2013) observed temporary excursions from the typical radio/X-ray correlation in BHXB GX 339-4 when measured over < 2 dex in X-ray luminosity.

Our measurement for EXO 1745–248 is much more consistent with 4U 1728–34, rather than Aql X-1 or the BHXBs (see Figure 3), where the EXO 1745–248 and 4U 1728–34 indices are what is expected from the model presented above for a radiatively efficient accretion flow coupled to a compact jet. Interestingly, Aql X-1 has (only once) shown evidence of X-ray pulsations (Casella et al.

⁹ In previous studies that compute the radio/X-ray correlation, the X-ray energy band used can vary from author to author, but in this work we choose the 1–10 keV band, as we have found that this band is most commonly used in recent literature; e.g., Gallo et al. 2014; Corbel et al. 2013; Deller et al. 2015.

¹⁰ In this work, all of our codes use the emcee python package to implement the MCMC algorithms (Hogg et al. 2010; Foreman-Mackey et al. 2013).

¹¹ Although this is a standard assumption in many papers, we point out two caveats for NSXBs. First, this assumes that the bolometric correction (in the hard state) remains constant so that the X-ray luminosity measured over limited energies is representative of the bolometric luminosity. Second, there may be multiple mass accretion rates (e.g., that in the disc versus that in a radial inflow) contributing to the X-ray luminosity of a NSXB, and it is unclear which of these would impact jet production.

¹² Hard X-ray colour is defined in Miller-Jones et al. (2010) as the count rate ratio between the 9.0–16.0 keV and 6.0–9.7 keV bands.

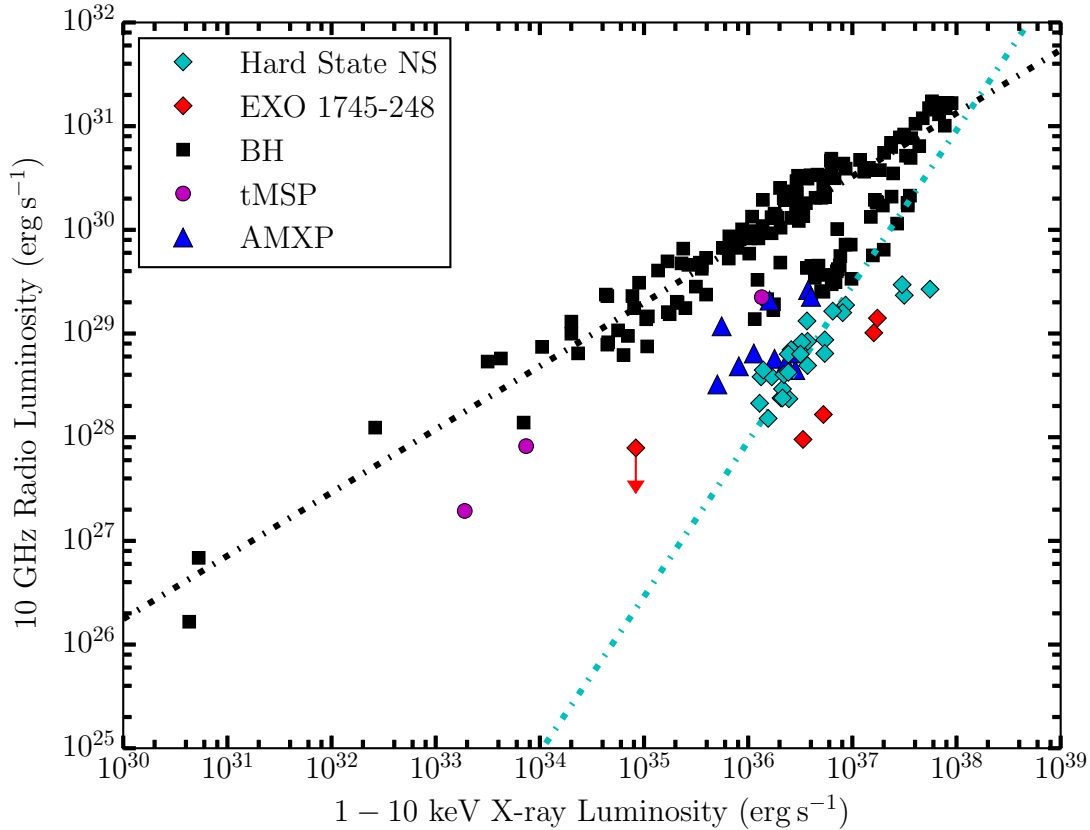


Figure 3. Radio/X-ray correlation for different types of accreting stellar mass compact objects. Data points from the literature include, BHs (Miller-Jones et al. 2011; Gallo et al. 2012; Ratti et al. 2012; Corbel et al. 2013; Gallo et al. 2014), hard state neutron stars (Migliari & Fender 2006; Miller-Jones et al. 2010), transitional binary milli-second pulsars (tMSPs) and accreting milli-second X-ray pulsars (AMXPs) (Hill et al. 2011; Papitto et al. 2013; Deller et al. 2015). Note that to convert between different radio bands we assume a flat radio spectral index. The dot-dashed lines show the best fit relations for BH ($\beta = 0.61$, black; Gallo et al. 2014) and hard state NS systems ($\beta = 1.40$, cyan; Migliari & Fender 2006). The new measurements of EXO 1745–248 reported in this paper (highlighted in red; luminosities assume a distance of 5.9 kpc) are more radio quiet and/or X-ray loud when compared with the other hard state NS measurements. Note that error bars are not included in this plot for clarity.

2008), suggesting that it may be more similar to the AMXPs or tMSPs.

Deller et al. (2015), recently combined radio and X-ray measurements for three tMSPs to fit a correlation of $L_R \propto L_X^{0.7}$ over ~ 3 dex in X-ray luminosity, which occupies a region of the radio/X-ray plane distinct from all the hard state NSXBs, like EXO 1745–248 (see Figure 3). Given that there is only one data point for this correlation in each individual tMSP, we are forced to only consider the correlation of this entire sample; although, given the correlation in BHXBs, we might expect the sample correlation to have a larger scatter than one might find in an individual source. The disc-jet coupling indices of tMSPs as a group are much more consistent with Aql X-1 than with EXO 1745–248 or 4U 1728–34. Deller et al. (2015) suggest that tMSPs are undergoing a propeller accretion mode, where the pressure of in-falling material is balanced by the magnetic field of the NS, and the NS’s rotation accelerates the inner disc, in turn causing the majority of the material to be ejected in outflows as opposed to falling inward. This theory can explain the radiatively inefficient jet dominated states seen at lower accretion rates in tMSPs (i.e. the tMSP correlation, $L_R \propto L_X^{0.7}$), which display a similar disc-jet coupling index as those of BHXBs, just at fainter radio luminosities (the offset between BHXBs and tMSPs

could be due to differing jet power, radiative efficiency, compact object mass, or jet launching mechanisms). However, it is unknown whether this jet dominated state occurs in all NSXBs or if entrance into this state is solely dependent on intrinsic NS characteristics such as magnetic field strength or spin period. In the current published NSXB sample (excluding tMSPs), only one correlation measurement (i.e., our lowest luminosity point in EXO 1745–248) probes X-ray luminosities $\lesssim 10^{35}$ erg s $^{-1}$. However, this measurement only has an upper limit on radio luminosity. While this data point appears not to be consistent with the tMSP correlation, we are unable to definitely determine whether this point lies on the extrapolation of our hard state NSXB best fit correlation at lower X-ray luminosities or perhaps, is part of an intermediate regime where the disc-jet coupling index flattens out during the transition between a steeper and flatter index (as seen in the multiple BHXBs, H1743–322; Coriat et al. 2011, XTE J1752–223; Ratti et al. 2012, and MAXI J1659–152; Jonker et al. 2012).

From Figure 3 it is also clear that EXO 1745–248 has a lower normalization compared to the other hard state NSs, Aql X-1 and 4U 1728–34, by about a factor of 5 in radio luminosity at the same X-ray luminosity. Among transient XBs measured in the hard state at $L_X > 10^{36}$ erg s $^{-1}$, EXO 1745–248 is the most ra-

dio faint source reported to date. This differing normalization may be analogous to what is seen in BH sources, where different individual sources appear to have different normalizations (Gallo et al. 2014). We note that while this difference could arise from having a well-known distance for EXO 1745–248 compared to more uncertain distances to Aql X-1 and 4U 1728–34, the distances to Aql X-1 and 4U 1728–34 would have to increase by a factor of three if this was a distance effect alone, which seems unlikely. On the other hand, a factor of 5 lower in radio luminosity at a given X-ray luminosity requires masses lower by a factor of about 10 if the sources follow the fundamental plane of BH accretion. Since NSs do not have such a large range of masses, mass alone can not explain the lower luminosity of EXO 1745–248, unless NSs and BHs follow very different fundamental planes of accretion. Further, Migliari et al. (2011) found a possible relation between spin frequency and jet power, with faster spinning neutron stars being more radio luminous. Based on its X-ray burst properties (§4.2), we expect EXO 1745–248 to have a typical spin (200–600 Hz). However, Migliari et al. (2011) did not include the recent results from tMSPs. At $L_X \sim 10^{36}$ erg s⁻¹, the tMSP M28I (254 Hz; Papitto et al. 2013) has a significantly higher radio luminosity than Aql X-1 (550 Hz; Watts et al. 2008). While this compares a tMSP to a NS, we take this as evidence that spin alone also cannot explain how radio loud a NSXB will be. Thus it seems likely that a combination of factors (e.g., mass, spin, inclination, magnetic field, radiative efficiency) may be required to produce a given radio luminosity.

This highlights the need for more radio/X-ray measurements of NSXBs, especially at the lower end of the luminosity spectrum, to answer these open questions. However, we note that obtaining such observations is very difficult, given that these NSXB sources decay very quickly (timescales on the order of a few days) through this desired luminosity range of $10^{34} - 10^{36}$ erg s⁻¹, necessitating intensive monitoring of these sources.

4.2 X-ray Burst Analysis

During our analysis we observed the presence of an X-ray burst, which we use here to further constrain the properties of this NSXB. Swift XRT detected an X-ray burst from Terzan 5 on 2015 Mar 25, with a net peak count rate at 04:56:42 UT of about 120 cnts s⁻¹ (0.5–10 keV), on top of the persistent emission (~ 10 cnts s⁻¹). From the 0.5 s time-resolution light curve we estimate a rise time of 1.8 s (defined as the time to go from 25% to 90% of the net peak count rate). The burst lasted for about 25 s and then reached a “plateau” for another ~ 25 s, at a level higher than the pre-burst count rate. About 50 s after the burst onset the observation was interrupted (see Figure 4).

To study the spectral evolution of the X-ray burst, we extracted a series of 3 s-long spectra from WT XRT data, using a 100 s interval before the burst to subtract the persistent (source plus background) emission. We used a 20-pixel radius region to extract the spectra, and verified that excluding the innermost 2 pixels (to correct for potential pile up) leads to consistent results. We created an exposure map and ancillary response file and used the latest response matrix from the calibration database. We grouped the resulting spectra to a minimum of 5 counts per channel, and fitted those spectra with more than 50 net counts in total with an absorbed blackbody model (TBABS*BBODYRAD in XSPEC, with the column density frozen at the value derived from the persistent emission; 3×10^{22} cm⁻²).

We find a slow decay in temperature along the burst decay (“cooling tail”), from ~ 2.9 keV to ~ 1.4 keV, identifying this un-

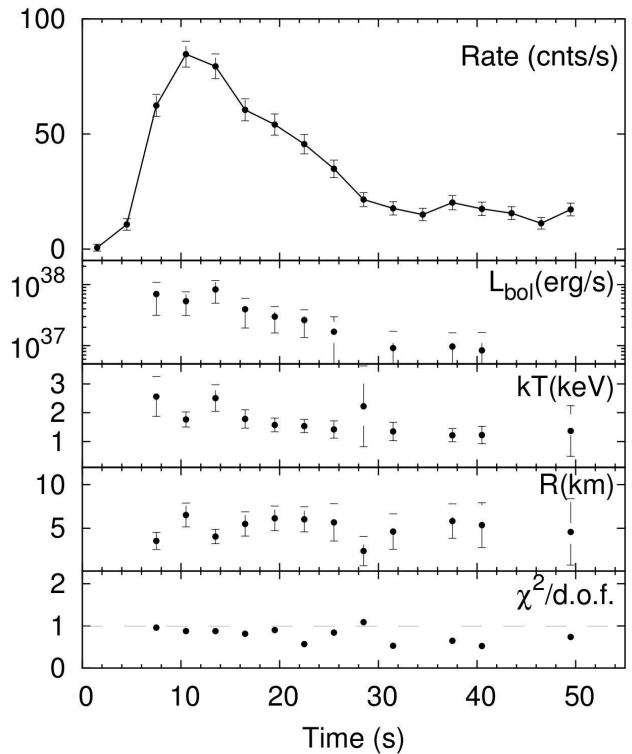


Figure 4. Time-resolved spectroscopy of the detected type-I X-ray burst. An absorbed blackbody model was used to fit the data. We found evidence indicating slow cooling during the burst decay, however we found no evidence of photospheric radius expansion. Panels from top to bottom: Swift/XRT count rate, bolometric luminosity, temperature, apparent radius, reduced chi-squared of the spectral fit.

equivocally as a thermonuclear event. The burst bolometric peak luminosity was $(10 \pm 4) \times 10^{37}$ erg s⁻¹, the apparent emitting radius between 3 and 5 km (without color or redshift corrections), and the total radiated energy about 1.0×10^{39} erg (see Figure 4). The persistent (0.5–10 keV) luminosity during the observation where the burst occurred was $(5.6 \pm 0.1) \times 10^{36}$ erg s⁻¹ (about 5% of the Eddington limit for a bolometric correction factor of 2 and $L_{\text{Edd}} = 2.5 \times 10^{38}$ erg s⁻¹).

The peak of the 2015 outburst occurred on Apr 22, at about ten times higher L_X , i.e., not far from 50% L_{Edd} (for a $1.4 M_{\odot}$ NS). Despite good Swift coverage (~ 5 ksec) of the following two weeks, when L_X dropped by about a factor 2, no other bursts were detected. This burst behaviour resembles that of most thermonuclear bursters, where bursts virtually disappear at mass accretion rates above 10% Eddington.

A second burster in Terzan 5, IGR 17480-2446, displays drastically different behaviour, namely a copious number of thermonuclear bursts at mass accretion rates between 10% and 50% Eddington (Linares et al. 2012). The atypical behaviour in IGR J17480-2446 has been attributed to its slow (11 Hz) spin (Cavecchi et al. 2011; Linares et al. 2012). Under this interpretation, the typical bursting behaviour of EXO 1745-248 would imply that it contains a rapidly rotating neutron star ($\sim 200 - 600$ Hz), like most low-mass NSXBs.

Galloway et al. (2008) define a burst timescale as $\tau = E_{\text{Burst}}/F_{\text{Peak}}$, where E_{Burst} is the total fluence during the burst and

F_{Peak} is the peak flux of the burst. Following their definition, we find a burst timescale of ≈ 22 s for EXO 1745–248. The 21 bursts seen by RXTE early in the 2000 outburst of EXO 1745–248 showed long burst durations ($\tau \sim 25$ s) and other characteristics of H burning. However, two bursts seen later in the outburst were shorter ($\tau \sim 10$ s), suggesting pure He (the explanation of this change in behaviour is not clear; Galloway et al. 2008). Therefore, we conclude that the measured timescale of this burst indicates the donor is likely hydrogen-rich.

5 CONCLUSIONS

In this paper, we present the results of our observations of the Terzan 5 NSXB EXO 1745–248 during its 2015 outburst at radio and X-ray frequencies, with the VLA, ATCA, and Swift XRT. Our (near-) simultaneous radio and X-ray measurements, all taken during the hard accretion state, allow us to construct and fit the radio/X-ray correlation for this source ($L_R \propto L_X^\beta$; β represents the disc-jet coupling index), which links the accretion flow to the relativistic jet in XBs. In contrast to the multiple BHXBs with a measured correlation, only two NSXBs have a measured radio/X-ray correlation, Aql X-1 ($L_R \propto L_X^{0.76}$) and 4U 1728–34 ($L_R \propto L_X^{1.5}$). Additionally, an ensemble of tMSPs has been shown to follow a correlation, $L_R \propto L_X^{0.7}$, much more consistent with BHXBs. As such, more measurements from NSXBs are needed to disentangle the different correlations. This work marks the third NSXB where the radio/X-ray correlation is measured in a single source, and the first where the distance is well known.

To fit the radio/X-ray correlation in EXO 1745–248 we developed a new MCMC based technique. We find a best fit normalization and disc-jet coupling index for the radio/X-ray correlation in EXO 1745–248 of $\xi = 0.94^{+0.14}_{-0.13}$ and $\beta = 1.68^{+0.10}_{-0.09}$, respectively, where $(\log L_R - \log L_{R,c}) = \log \xi + \beta(\log L_X - \log L_{X,c})$, with centering values $L_{R,c} = 3.89 \times 10^{28}$ erg s $^{-1}$ and $L_{X,c} = 8.38 \times 10^{36}$ erg s $^{-1}$.

This disc-jet coupling index is consistent with what we would expect for a compact jet coupled to a radiatively efficient accretion flow (presumably due to the NSs surface), rather than a radiatively inefficient flow (as thought to exist in most BHXBs and possibly tMSPs). Empirically this index is consistent with the index for NSXB 4U 1728–34, but inconsistent with our measured index for NSXB Aql X-1. Therefore, a similar radio/X-ray correlation in the hard accretion state does not appear to hold across all three NSXBs measured so far, as it does in the BHXB population. However, all three NSXB correlations are measured over a smaller lever arm in X-ray luminosity (~ 1 dex) when compared to BHXBs.

Notably, we find that EXO 1745–248 is much more radio faint when compared to 4U 1728–34 and Aql X-1, where neither distance, mass, or spin considerations alone appear to be able to account for the discrepancy.

Finally, we detected an X-ray burst during this outburst. Through performing time-resolved spectral analysis, we find evidence of cooling during the decay of this burst and that the burst timescale is consistent with hydrogen burning, suggesting that this was a hydrogen Type-I X-ray burst.

ACKNOWLEDGEMENTS

AJT would like to thank Erik Rosolowsky for helpful discussions regarding MCMC implementation. AJT, GRS, and COH are supported by NSERC Discovery Grants. JCAMJ is the recipient of an

Australian Research Council Future Fellowship (FT140101082). ML was supported by the Spanish Ministry of Economy and Competitiveness under the grant AYA2013-42627. ET acknowledges support from NSF grant AST-1412549. JS acknowledges support via NSF grant AST-1308124. ND acknowledges support via an NWO/Vidi grant and an EU Marie Curie Intra-European fellowship under contract no. FP-PEOPLE-2013-IEF-627148. DA acknowledges support from the Royal Society. AP acknowledges support from an NWO Vidi fellowship. RW is supported by a NWO Top Grant, Module 1. The National Radio Astronomy Observatory is a facility of the National Science Foundation operated under cooperative agreement by Associated Universities, Inc. This research has made use of the following data and software packages: Swift BAT transient monitor results provided by the Swift BAT team, and the Swift XRT Data Analysis Software (XRTDAS) developed under the responsibility of the ASI Science Data Center (ASDC), Italy. We acknowledge extensive use of the ADS and arXiv.

REFERENCES

- Altamirano D., et al., 2012a, MNRAS, 426, 927
 Altamirano D., et al., 2012b, MNRAS, 426, 927
 Altamirano D., H.A. K., Patruno A., Bahramian A., Heinke C., Wijnands R., Degenaar N., 2015, ATel, 7240, 1
 Arnaud K., 1996, n ASP Conf. Ser. 101: Astronomical Data Analysis Software and Systems V XSPEC: The First Ten Years., 17
 Bahramian A., Heinke C., Sivakoff G., Gladstone J. C., 2013, ApJ, 766, 10
 Bahramian A., et al., 2014, ApJ, 780, 127
 Bahramian A., et al., 2015, ATel, 7242, 1
 Blackburn J., 1995, in Shaw R. A., Payne H. E., Hayes J. J. E., eds, Astronomical Data Analysis Software and Systems IV Vol. 77 of Astronomical Society of the Pacific Conference Series, FTOOLS: A FITS Data Processing and Analysis Software Package, 367
 Blandford R. D., Konigl A., 1979, ApJ, 232, 34
 Bordas P., et al., 2010, ATel, 2929, 1
 Casella P., Altamirano D., Patruno A., Wijnands R., van der Klis M., 2008, ApJ, 674, L41
 Cavecchi Y., et al., 2011, ApJ, 740, L8
 Corbel S., Nowak M., Fender R., Tzioumis T., Markoff S., 2003, A&A, 400, 1007
 Corbel S., Coriat M., Brocksopp C., Tzioumis A., Fender R., Tomsick J. A., M.M. B., Bailyn C., 2013, MNRAS, 428, 2500
 Coriat M., et al., 2011, MNRAS, 414, 677
 Degenaar N., Wijnands R., 2012, MNRAS, 422, 581
 Deller A. T., et al., 2015, ApJ, 809, 13
 Falcke H., Biermann P., 1995, A&A, 293, 665
 Falcke H., Kording E., Markoff S., 2004, A&A, 414, 895
 Fender R., Kuulkers E., 2001, MNRAS, 324, 923
 Fender R., Hjellming R., Tilanus R., Pooley G., Deane J., Ogle R., Spencer R., 2001, MNRAS, 322, L23
 Fender R., Belloni T., Gallo E., 2004a, MNRAS, 355, 1105
 Fender R., Wu K., Johnson H., Tzioumis T., Jonker P., Spencer R., van der Klis M., 2004b, Nature, 427, 222
 Fender R., Homan J., Belloni T., 2009, MNRAS, 396, 1370
 Ferraro F., Pallanca C., Lanzoni B., Cadelano M., Massari D., Dalessandro E., Mucciareli A., 2015, ApJ, 807, L1
 Fomalont E., Geldzahler B. J., Bradshaw C., 2001, ApJ, 558, 283
 Foreman-Mackey D., Hogg D. W., Lang D., Goodman J., 2013, PASP, 125, 306
 Gallo E., Fender R. P., Pooley G., 2003, MNRAS, 344, 60
 Gallo E., Miller B., Fender R., 2012, MNRAS, 423, 590
 Gallo E., et al., 2014, MNRAS, 445, 290
 Galloway D., Muno M. P. amd Hartman J., Psaltis D., Chakrabarty D., 2008, ApJSS, 179, 360

- Heinke C., Edmonds P., Grindlay J. E., Lloyd D., Cohn H., Lugger P., 2003, *ApJ*, 590, 809
- Heinke C., Wijnands R., Cohn H. N., Lugger P. M., Grindlay J. E., Pooley D., Lewin W. H. G., 2006, *ApJ*, 651, 1098
- Heinz S., Sunyaev R., 2003, *MNRAS*, 343, L59
- Hill A. B., et al., 2011, *MNRAS*, 415, 235
- Hogg D., Bovy J., Lang D., 2010, arXiv:1008.4686
- Homan J., et al., 2010, *ApJ*, 719, 201
- Inoue H., et al., 1984, *PASJ*, 36, 855
- Jonker P., Miller-Jones J., Homan J., Tomsick J., Fender R., Kaaret P., Markoff S. B., Gallo E., 2012, *MNRAS*, 423, 3308
- Kalemci E., Dincer T., Tomsick J., Buxton M., Bailyn C., Chun Y., 2013, *ApJ*, 779, 14
- Kording E., Fender R., Migliari S., 2006, *MNRAS*, 369, 1451
- Krimm H. A., et al., 2013, *ApJSS*, 209, 14
- Kuulkers E., den Hartog P. R., in 't Zand J. J. M., Verbunt F., Harris W., Cocchi M., 2003, *A&A*, 399, 663
- Lanzoni B., et al., 2010, *ApJ*, 717, 653
- Linares M., Altamirano D., Chakrabarty D., Cumming A., Keek L., 2012, *ApJ*, 748, 13
- Linares M., et al., 2015, *ATel*, 7247, 1
- Maccarone T., 2003, *A&A*, 409, 697
- Makishima K., et al., 1981, *ApJ*, 247, L23
- Markoff S., Nowak M., Corbel S., Fender R., Falcke H., 2003, *A&A*, 397
- McMullin J. P., Waters B., Schiebel D., Young W., Golap K., 2007, *Astronomical Data Analysis Software and Systems XVI*, ed. R.A. Shaw, F. Hill and D.J. Bell, *Astronomical Society of the Pacific Conference Series*, Volume 376, 127
- Merloni A., Heinz S., Di Matteo T., 2003, *MNRAS*, 345, 1057
- Migliari S., Fender R., 2006, *MNRAS*, 366, 79
- Migliari S., Fender R. P., Rupen M., Jonker P. G., Klein-Wolt M., Hjellming R. M., van der Klis M., 2003, *MNRAS*, 342, L67
- Migliari S., Fender R., Rupen M., Wachter S., Jonker P., Homan J., van der Klis M., 2004, *MNRAS*, 351, 186
- Migliari S., et al., 2010, *ApJ*, 710, 117
- Migliari S., Miller-Jones J. C. A., Russell D. M., 2011, *MNRAS*, 415, 2407
- Miller-Jones J. C. A., et al., 2010, *MNRAS*, 407, L109
- Miller-Jones J. C. A., Jonker P., Maccarone T., Nelemans G., Calvelo D. E., 2011, *ApJ*, 739, L18
- Miller-Jones J. C. A., et al., 2012, *MNRAS*, 421, 468
- Papitto A., et al., 2013, *Nature*, 501, 517
- Plotkin R., Markoff S., Kelly B., Kording E., Anderson S., 2012, *MNRAS*, 419, 267
- Plotkin R. M., et al., 2015, *MNRAS Accepted*, arXiv: 1512.01941
- Ratti E. M., et al., 2012, *MNRAS*, 423, 2656
- Sault R., Teuben P., Wright M., 1995, *Astronomical Data Analysis Software and Systems IV*, *Astronomical Society of the Pacific Conference Series* Volume 77, 433
- Serino M., Mihara T., Matsuoka M., Nakahira S., Sugizaki M., Ueda Y., Kawai N., Ueno S., 2012, *PASJ*, 64, 5
- Spencer R., Rushton A. P., Balucinska-Church M., Paragi Z., Schulz N., Wilms J., Pooley G., Church M., 2013, *MNRAS*, 435, L48
- Strohmayer T. E., Markwardt C. B., 2010, *ATEL*, 2569, 1
- Tananbaum H., Gursky H., Kellogg E., Giacconi R., 1972, *ApJ*, 177, L5
- Tetarenko B., Sivakoff G., Heinke C., Gladstone J. C., 2016, *ApJS*, 222, 15
- Tremou E., et al., 2015, *ATel*, 7262, 1
- Tudose V., Fender R. P., Linares M., Maitra D., van der Klis M., 2009, *MNRAS*, 400, 2111
- Vadawale S. V., Rao A. R., Naik S., Yadav J. S., Ishwara-Chandra C. H., R.A. P., Pooley G. G., 2003, *ApJ*, 597, 1023
- Valenti E., Ferraro F., Origlia L., 2007, *AJ*, 133, 1287
- Verner D. A., Ferland G. J., Korista K. T., Yakovlev D. G., 1996, *ApJ*, 465, 487
- Watts A., Krishnan B., Bildsten L., Schutz F., 2008, *MNRAS*, 389, 839
- Wijnands R., Heinke C., Pooley D., Edmonds P., Lewin W., Grindlay J., Jonker P., Miller J. M., 2005, *ApJ*, 618, 883
- Wilms J., Allen A., McCray R., 2000, *ApJ*, 542, 914

This paper has been typeset from a $\text{\TeX}/\text{\LaTeX}$ file prepared by the author.